Polymer Degradation and Stability 95 (2010) 2328–2333

Contents lists available at ScienceDirect

Polymer Degradation and Stability

journal homepage: www.elsevier.com/locate/polydegstab

# Effect of amine groups on the synthesis and antibacterial performance of Ag nanoparticles dispersed in aminosilanes-modified silicate

K.H. Wu [a,*], Y.C. Chang [a], W.Y. Tsai [a], M.Y. Huang [a], C.C. Yang [b]

[a] Department of Chemistry and Material Engineering, Chung Cheng Institute of Technology, NDU, Tahsi, Taoyuan 335, Taiwan
[b] Chemical Systems Research Division, Chung Shan Institute of Science and Technology, Lungtan, Taoyuan 325, Taiwan

ARTICLE INFO

*Article history:*
Received 21 June 2010
Received in revised form
20 August 2010
Accepted 28 August 2010
Available online 15 September 2010

*Keywords:*
Polymer–matrix composites
Silver (Ag)
Organically-modified silicate
Antibacterial performance

ABSTRACT

Nanocomposites based on silver (Ag) and organically-modified silicate (Ormosil) were prepared by an *in situ* reduction method, in which silver nitrate, tetraethoxysilane (TEOS) and aminosilanes with different amine groups acted as precursor, linker and colloidal suspension stabilizers, respectively. The objective of the study was to develop and evaluate aminosilanes-modified silicate impregnated with Ag nanoparticles, in which Ag dispersion is stabilized, to create a composite that protects against biological warfare agents. The physical properties of the Ormosil/Ag nanocomposites were examined using NMR, ESR and SEM spectroscopy, the results of which indicated that the extent of the reduction reaction increases with aminosilanes with a higher number of amine groups. The number of amine groups in the aminosilane has also a strong effect on the size of the resulting Ag particles. The antibacterial effects of the Ormosil/Ag nanocomposites were assessed by the zone of inhibition and plate-counting methods, and an excellent antibacterial performance was discovered.



## 1. Introduction

Organically-modified silicates (Ormosils) are hybrid organic–inorganic materials formed through by hydrolysis and condensation of organically-modified silanes with traditional alkoxide precursors. Ormosil materials represent an important area of research in materials science, as they have already been found to have many promising applications in the fields of optics, electronics, ionics, mechanics, energy, environment, biology and medicine [1–3]. Such versatility arises from combining the benefits and desirable properties of both constituents, inorganic (e.g., mechanical and thermal stability) and organic (e.g., flexibility and functionality) [4]. Ormosils have been shown to be excellent hosts for trapping nanoparticles of metals and semiconductors [5–8] because of their ability to act as stabilizers or surface capping agents. When nanoparticles are embedded or encapsulated in an Ormosil, the Ormosil terminates the growth of the particles by controlling nucleation [9].

Silver-based antimicrobials are a subject of much attention, not only because of the non-toxicity of active $Ag^+$ to human cells [10], but also because of their novel properties as long-lasting biocides with high-temperature stability and low volatility. The antimicrobial activity of silver ions has been well established [11]. Silver ions are significant antimicrobials by virtue of their antiseptic properties [12], with only a few bacteria being intrinsically resistant to this metal [13], and silver is well known as a significant resource for topical therapy owing to its beneficial antimicrobial properties in medical devices such as catheters, cannulae, etc. [14,15]. In addition, nanosilver has excellent properties of conformational entropy in polyvalent binding [16,17], which make attachment to flexible polymeric chains of antibiotics easy. Moreover, nanosilver exhibits chemical stability and is of an appropriate size, with well-developed surface chemistry.

In order to obtain high-performance materials, it is extremely important that the particle size and structure can be controlled. One significant approach is to synthesize materials in the presence of a porous solid, such as alumina, polymer matrices and mesoporous silica. There have been a number of reports of the synthesis of silver nanoparticles in polymers, rendering variation in physical, chemical and optical properties possible depending on the polymer itself. The protection of silver nanoparticles by polymers such as poly(vinylalcohol) (PVA) [18], poly(vinylpyrolidone) (PVP) [19], polystyrene (PS) or poly(ethyleneimine) (PEI) [20], poly(ethylene glycol) (PEG) [21], polyurethane (PU) [22], polyaniline (PANI) [23] and poly(vinylalcohol)/poly(ethyleneimine) (PVA/PEI) [24] has been extensively reported, but though there have been several reports [6,9,25,26] of silver-doped classical sol–gel silicate glass, research into the silver-doping of Ormosils, in which tetraethoxysilane

* Corresponding author.
*E-mail address:* khwu@ndu.edu.tw (K.H. Wu).

0141-3910/$ – see front matter © 2010 Elsevier Ltd. All rights reserved.
doi:10.1016/j.polymdegradstab.2010.08.025

(TEOS) and aminosilanes act as the inorganic and organic components, respectively, remains scarce.

In this study, we developed a simple method for immobilizing Ag in an aminosilanes-modified silicate hybrid to facilitate transport of Ormosil/Ag through membranes and investigated the microstructure, physical properties and antibacterial activity of the resulting composites. Ag nanoparticles were obtained by chemical reduction of $AgNO_3$ in hydrazine using aminosilanes as colloidal suspension stabilizers. The reaction was performed using aminosilanes with different amine groups in water in order to achieve nanoparticles isolation and a stable colloidal suspension, and to control the size. Zone of inhibition testing and the plate-counting method were used in this study to examine the antibacterial activity of the Ormosil/Ag nanocomposites against Gram-negative *Escherichia coli* (*E. coli*) and *Pseudomonas aeruginosa* (*P. aeruginosa*), and Gram-positive *Staphylococcus aureus* (*S. aureus*) and *Bacillus subtilis* (*B. subtilis*).

## 2. Experimental

### 2.1. Preparation of the Ormosil/Ag nanocomposites

The Ag-doped Ormosil nanocomposites were prepared as shown in Fig. 1. An acid-catalyzed process, using *N*-[3-(trimethoxysilyl)propyl]diethylenetriamine (ATS), 3-(2-aminoethylaminopropyl) trimethoxysilane (AES) and tetraethoxysilane (TEOS) as the precursors, was employed to prepare the Ormosil(ATS) and Ormosil (AES) solution. The reagents were purchased from Aldrich and were used as received. TEOS and ATS or AES were placed in a beaker with 0.05 M $HNO_3$. Ormosil(ATS) was prepared using 0.02 mol of TEOS, 0.02 mol of ATS, and deionized water, and the sol was stirred for 2 days before the addition of $AgNO_3$ solution. Quantitative $AgNO_3$ (weight ratio 1:0.05 with respect to ATS + TEOS) was dissolved into 50 ml aqueous dispersion solution containing 10 wt.% $NH_3$. After stirring for 30 min, dilute aqueous solution of hydrazine monohydrate was introduced to the biamminesilver nitrate ($[Ag(NH_3)_2]NO_3$) solution in the appropriate quantity (molar ratio 1:1 with respect to silver nitrate) using a syringe. The resulting solution was added to the above-described sol solution, and stirring was continued under an inert atmosphere at room temperature for another 12 h. The sol solution was then cast onto a polytetrafluoroethylene plate and placed in a drying oven at 50 °C for 12 h, and the Ormosil(ATS)/Ag composite was finally obtained by heat-treating the dried films at 110 °C for 1 h. Ormosil(AES) hybrid and Ormosil(AES)/Ag composite films were prepared in the same way.

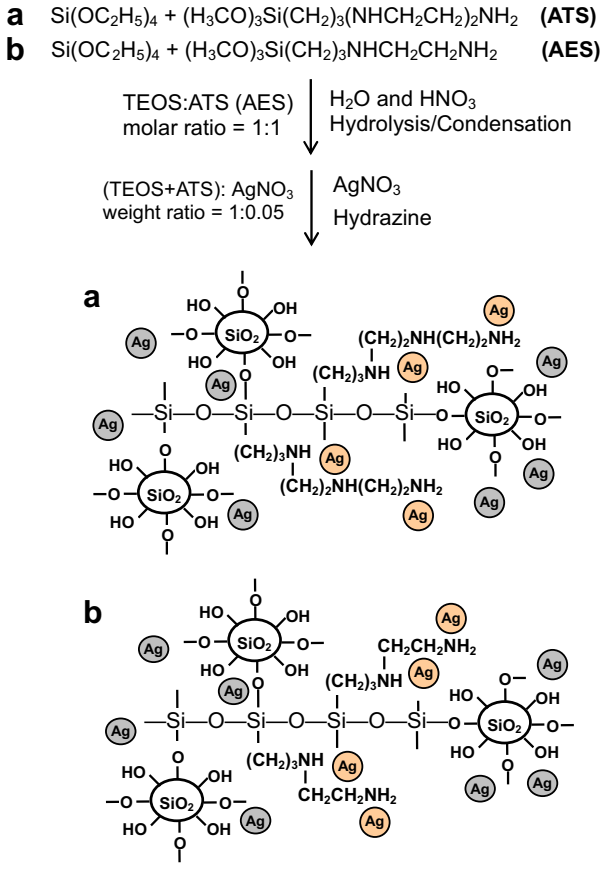


**Fig. 1.** Experimental procedure for the synthesis of (a) Ormosil(ATS)/Ag and (b) Ormosil(AES)/Ag nanocomposites.

### 2.2. Experimental techniques

Phase identification of the samples was performed using X-ray diffraction with Cu Kα radiation. $^{13}C$ and $^{29}Si$ NMR spectra of the solid-state sample were obtained (MSL-400, Bruker) by the cross-polarization/magic-angle spinning (CP–MAS) technique. The nomenclature of $T^i$ and $Q^i$ was taken from Glaser et al. [27]: $T^i$ and $Q^i$ denote species that have one and no organic side group, where $i$ refers to the number of –O–Si groups bound to the silicon atom of interest. The ESR spectra of the samples were recorded on a Bruker EMX-10 electron spin resonance spectrometer operating at the X-band ($\nu$ = 9.6 GHz) with 100-kHz field modulations. Diphenyl picrylic hydrazole (DPPH; $g$ = 2.0036) was used as a field marker. The morphology of the samples was observed using a scanning electron microscope (SEM, Hitachi S-800) and a transmission electron microscope (TEM, Philips CM-200) equipped with an energy-dispersive X-ray (EDX, Hitachi S-300) microanalysis system. A Perkin–Elmer thermal gravimetric analyzer (TGA-7) was used to investigate the thermal stability of the composites. The samples (about 10 mg) were heated in $N_2$ atmosphere from ambient temperature to 800 °C at a heating rate of 20 °C/min, and the gas flow rate was maintained at 50 mL/min.

### 2.3. Test of antibacterial properties

*P. aeruginosa* (ATCC 27853), *E. coli* (ATCC 25922), *S. aureus* (ATCC 25923), and *B. subtilis* (ATCC 43223) were obtained from the Food Industry Research and Development Institute, Taiwan, and were used as the reference strains in antibacterial testing. The antibacterial spectrum of the Ormosil/Ag composites was evaluated by zone of inhibition testing. A standard inoculum of the test organism with $10^7$ colony-forming units (CFU)/mL was swabbed onto the surface of a Muller–Hinton (MH) agar plate, and discs of filter paper impregnated with antibacterial agents (6 mg/mL) were placed on the agar. The plates were incubated overnight at 37 °C, and the clear zones around the disc were then measured.

The plate-counting method was used to further investigate the antibacterial effects of the composites [28]. Approximately $10^7$ CFU/mL of *S. aureus* were cultured on MH agar plates supplemented with the Ormosil/Ag composite. An Ormosil/Ag-free MH plate cultured under the same conditions was used as a control. The test process was as described as follows: 10–50 mg of the Ormosil/Ag composite was added to 3 mL of MH broth containing $10^7$ CFU/mL bacteria. The mixture was aerobically incubated at 37 °C under agitation for 24 h, and 30 μL of the above suspension was then cultured on an agar plate and incubated at 37 °C for 18 h. The bacterial concentrations were determined by measuring optical density (OD) at 600 nm. Then the OD values were changed into

concentration of *S. aureus* cells. The tests of zone of inhibition and plate-counting method were performed three times for each strain, and results in agreement on two or more occasions were adopted as the result of the strain. The counts on the three plates corresponding to a particular sample were averaged.

## 3. Results and discussion

### 3.1. Structure characterization

X-ray diffraction, solid-state $^{13}C$ and $^{29}Si$ NMR, and ESR provided evidence of the formation of Ormosil/Ag composites. Fig. 2 shows the XRD patterns of the Ormosil(AES)/Ag and the Ormosil(ATS)/Ag composites. The broad diffraction peaks near $2\theta = 12^\circ$ and $23^\circ$ were due to the amorphous phase of Ormosil. The XRD spectra of the Ormosil/Ag composites were in good agreement with the values for silver nanoparticles in the literature [29]: prominent peaks at $2\theta$ values of about 38, 44, 65 and 77 represented the (1 1 1), (2 0 0), (2 2 0) and (3 1 1) Bragg reflections of face-centered cubic crystalline silver. Furthermore, increasing the number of amine groups in aminosilanes induced the obvious enhancement of the characteristic peaks of silver, implying the development of larger and highly crystalline silver nanoparticles. The size of the nano-Ag grains ($2\theta = 38^\circ$) was estimated using Scherrer's formula, $D = 0.9\lambda/\beta\cos\theta$, where $D$ is the crystallite size in nm, $\lambda$ is the radiation wavelength (0.154056 nm for Cu $K_\alpha$), $\beta$ is the bandwidth at half-height and $\theta$ is the diffraction peak angle [30], and the calculated crystallite sizes were in the range of 10–30 nm.

$^{13}C$ and $^{29}Si$ CP–MAS NMR spectra were obtained for the Ormosil and the Ormosil/Ag composites as shown in Figs. 3 and 4. Distinct peaks were observed for Ormosil(AES) in the $^{13}C$ NMR spectra at 11.7 ($Si-CH_2CH_2$), 24.2 ($Si-CH_2CH_2CH_2$), 42.6 [$Si-(CH_2)_3NHCH_2CH_2NH_2$] and 53.2 ppm [$Si-(CH_2)_2CH_2NHCH_2CH_2NH_2$]. The Ormosil(ATS) in the $^{13}C$ NMR spectra were observed at 11.7 ($Si-CH_2CH_2$), 22.9 ($Si-CH_2CH_2CH_2$), 41.4 ($Si-CH_2CH_2CH_2NH$), 49.3 [$Si-CH_2(CH_2CH_2NH)_2CH_2CH_2NH_2$] and 51.8 ppm [$Si-(CH_2)_3NHCH_2CH_2NH(CH_2)_2NH_2$]. The signals in the $^{13}C$ NMR spectra of the Ormosil(AES)/Ag and Ormosil(ATS)/Ag composites partially overlapped, and the intensities were weakened by the incorporation of Ag. The result was due to dipolar interactions between $^{13}C$ nuclei and the paramagnetic Ag, which provided efficient NMR relaxation sinks. Moreover, two new characteristic peaks were observed at 30 and 32 ppm, indicating that the local environments of the C atoms in the Ormosil/Ag composites had changed. This result is very important because it proves that Ag particles formation on the amine groups in aminosilane occurred, which produced chelation or adsorption on the surface of aminosilane ($CH_2NH\ldots Ag$).

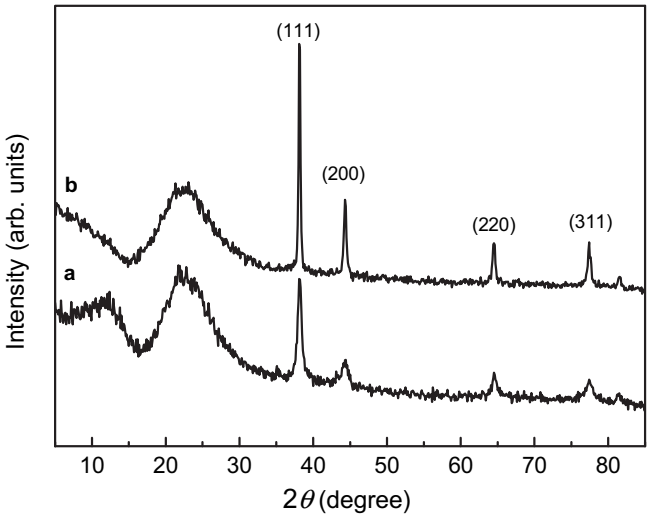


**Fig. 2.** XRD spectra of (a) Ormosil(AES)/Ag and (b) Ormosil(ATS)/Ag nanocomposite.

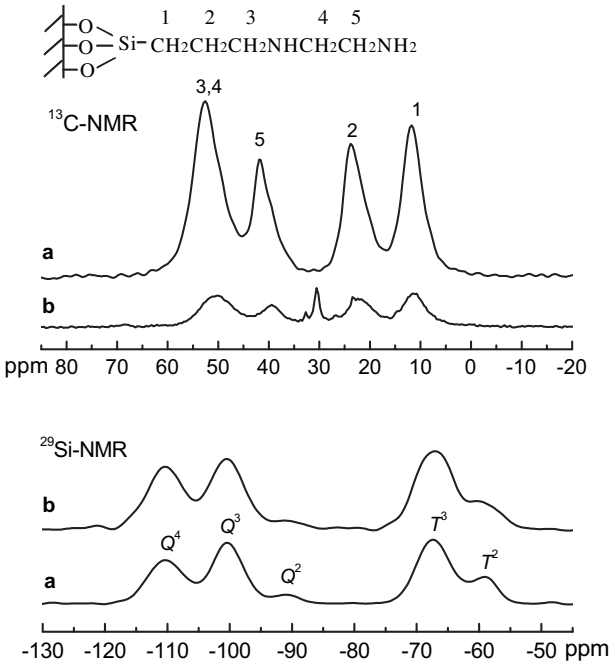


**Fig. 3.** $^{13}C$ and $^{29}Si$ CP/MAS NMR spectra of (a) Ormosil(AES) and (b) Ormosil(AES)/Ag nanocomposite.

Distinct peaks of the silica network units in the Ormosil(AES) and Ormosil(ATS) were observed at −59.0 ($T^2$), −67.4 ($T^3$), −90.9 ($Q^2$), −100.4 ($Q^3$) and −110.3 ppm ($Q^4$). $T^2$, $T^3$, $Q^2$, $Q^3$ and $Q^4$ denote $R-Si(OSi)_2(OH)$, $R-Si(OSi)_3$, $Si(OSi)_2(OH)_2$, $Si(OSi)_3(OH)$ and $Si(OSi)_4$, respectively. Moreover, the structural characterization of the

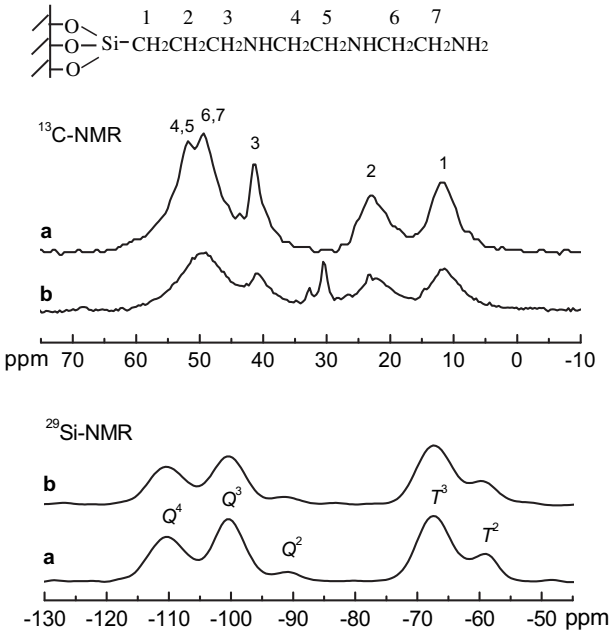


**Fig. 4.** $^{13}C$ and $^{29}Si$ CP/MAS NMR spectra of (a) Ormosil(ATS) and (b) Ormosil(ATS)/Ag nanocomposite.

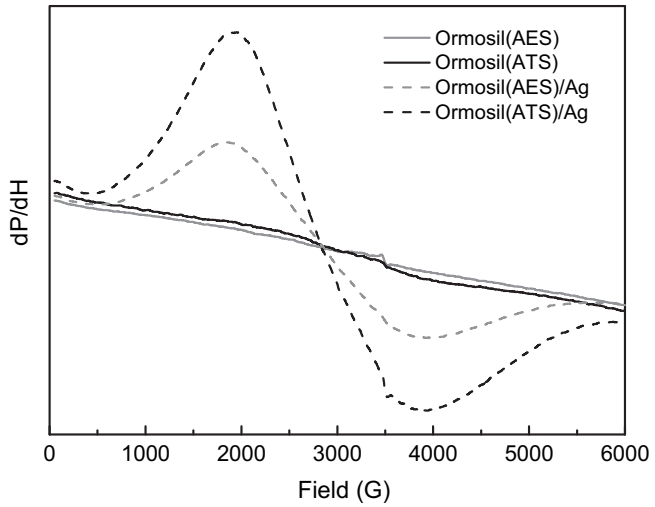


**Fig. 5.** ESR spectra of the Ormosil and the Ormosil/Ag nanocomposites obtained at room temperature.

Ormosil/Ag composites were in agreement with the Ormosil hybrids expected from the $^{29}$Si NMR spectra. However, the intensity ratios of $Q^4/Q^3$ and $T^3/T^2$ of the Ormosil(AES)/Ag composite ($Q^4/Q^3 = 0.915$; $T^3/T^2 = 2.628$) were larger than those of the Ormosil (AES) ($Q^4/Q^3 = 0.754$; $T^3/T^2 = 2.282$). The Ormosil(ATS)/Ag composite has also the same results. These results indicate that the Ag nanoparticles were coordinated with silica network units (Si–OH…Ag) and the intensity ratios of $Q^4$ and $T^3$ were therefore enhanced.

The ESR spectra of the Ormosil/Ag composites were recorded at room temperature, and the dependence of the number of amine groups in aminosilanes is shown in Fig. 5. The Ormosil/Ag composites included single-phase Ag with a crystalline structure, but in the Ormosil(AES) and the Ormosil(ATS) spectra the peak corresponding to the Ag phase was not observed. The intensity of the ESR signal, which is due to unpaired electrons, for Ormosil/Ag composites increases with aminosilanes with a higher number of amine groups. The number of amine groups in the aminosilane has a strong effect on the formation of the resulting Ag particles. Amine groups can be attributed a key role in the reduction of $Ag^+$. And this may be due to the coordination between N and $Ag^+$, which may decrease the potential of $Ag^+/Ag$ ($E_{Ag+/Ag}$) and promote the reduction of $Ag^+$ [9].

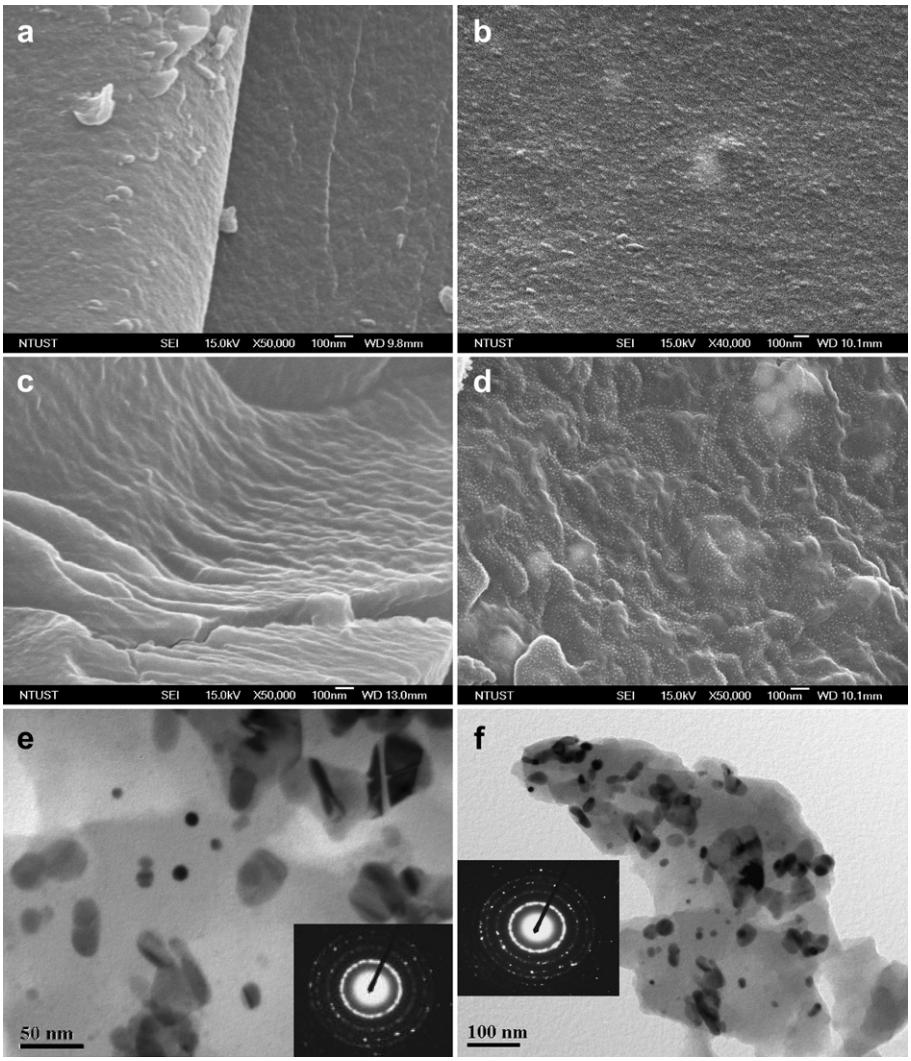


**Fig. 6.** SEM photographs of (a) Ormosil(AES), (b) Ormosil(AES)/Ag, (c) Ormosil(ATS) and (d) Ormosil(ATS)/Ag; TEM photographs of (e) Ormosil(AES)/Ag and (f) the Ormosil(ATS)/Ag.

### 3.2. Morphological and thermal analysis

SEM and TEM images were used to evaluate the surface morphology and size distribution of the Ag deposited in the Ormosil. The SEM image of the Ormosil hybrids exhibited a homogeneous morphology and the crosslinking density formed by the condensation reaction between molecular chains increased (Fig. 6a and c). On the other hand, it was observed that the Ormosil/Ag composites consisted of non-agglomerated, uniformly-distributed Ag particles in the Ormosil matrix (Fig. 6b and d). The TEM images of the Ormosil/Ag composites showed non-agglomerated, scattered spherical Ag particles at a high concentration, of sizes in the range of less than 50 nm (Fig. 6e and f). The electron diffraction pattern of the Ag nanoparticles demonstrated the superposition of the ring, as well as a spot pattern, which suggested the presence of both polycrystals and monocrystals [24]. In comparison with those of Ag particles, the SEM and TEM images of Ormosil/Ag, Polymer/Ag [24] and BC/Ag [31] vary greatly. The particle size of Ag in the Ormosil/Ag composite (<50 nm) was smaller than that in the BC/Ag (200 nm) and is more uniformly-distributed than that observed in a polymer (PVA/PEI) matrix [24]. This behavior could be attributed to the action of aminosilanes-modified silicate (Ormosil) as a surface modifier that inhibits Ag particle growth and prevents aggregation.

The weight-loss curves (TGA) and differential thermogravimetry (DTG) of the Ormosil and the Ormosil/Ag composites, obtained at a heating rate of 20 °C/min under nitrogen, are shown in Fig. 7. The degradation process of Ormosil(AES) is similar to that of Ormosil (ATS). However, the extent of the physical adsorption of water increased when the number of amine groups is greater in the aminosilane (ATS). Thus, the rate of scission of the ATS is larger than that of the AES. The weight loss observed below 200 °C was due to the physical adsorption and hydrogen bonding of water in the samples, while that between 200 and 400 °C was attributed to the decomposition of aliphatic amine segments linking the aminosilane units to the silica network, and the major mass loss observed at 400–700 °C was attributed to the decomposition of the silica network ($T^i$ and $Q^i$). Generally, the thermal stability of the Ormosil was enhanced by the inclusion of Ag nanoparticles. The thermal decomposition temperatures were enhanced for the Ormosil/Ag composites, and the Ormosil(AES)/Ag showed better thermal stability than the Ormosil(ATS)/Ag composite.

The DTG curves show that Ag weakened the rate of scission of aminosilane chains in Ormosil(AES)/Ag and Ormosil(ATS)/Ag composites, while the rate of the silica network chains increased in Ormosil(ATS)/Ag composite. Amine groups played a key role in this result, possibly due to interaction between –NH groups and Ag particles. Such a consequence may be due to the enhancement of heat transfer as a result of the increase in mobility of the Ag, which leads to a decrease in scission of aminosilane chains, resulting in an increase in scission within the silica network chains. This result revealed that there was a greater Ag content of Ormosil(ATS)/Ag composite, corresponding to the data of the ESR.

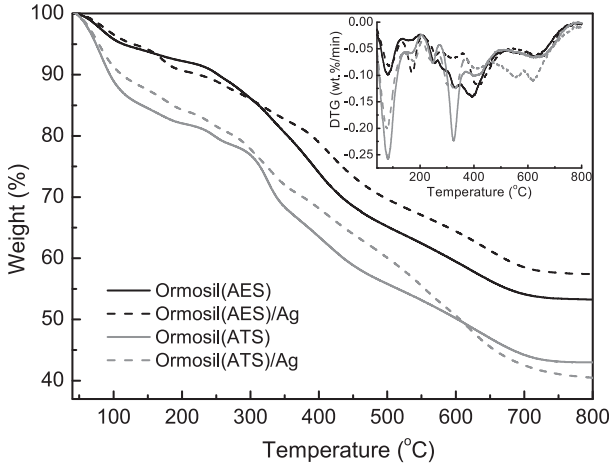


**Fig. 7.** TGA and DTG thermograms of the Ormosil and the Ormosil/Ag nanocomposites under nitrogen at the heating rate of 20 °C/min.

**Table 1**
Zone of inhibition (mm) against bacteria of the Ormosil and the Ormosil/Ag nanocomposites.

| Bacteria | Ormosil(ATS) | Ormosil(ATS)/Ag | Ormosil(AES) | Ormosil(AES)/Ag |
|---|---|---|---|---|
| *S. aureus* | 16.27 | 17.93 | 10.86 | 11.11 |
| *B. subtilis* | 26.39 | 30.09 | 8.62 | 15.03 |
| *E. coli* | 19.39 | 29.47 | 8.62 | 10.16 |
| *P. aeruginosa* | 20.68 | 24.03 | 8.62 | 9.32 |

### 3.3. Antibacterial effects

The antibacterial efficacies of the Ormosil/Ag composites against bacteria were assessed by zone of inhibition testing and the plate-counting method. Table 1 details the relative retention of activity (zone of inhibition) of the Ormosil and the Ormosil/Ag composites against bacteria. The Ormosil and the Ormosil/Ag composites

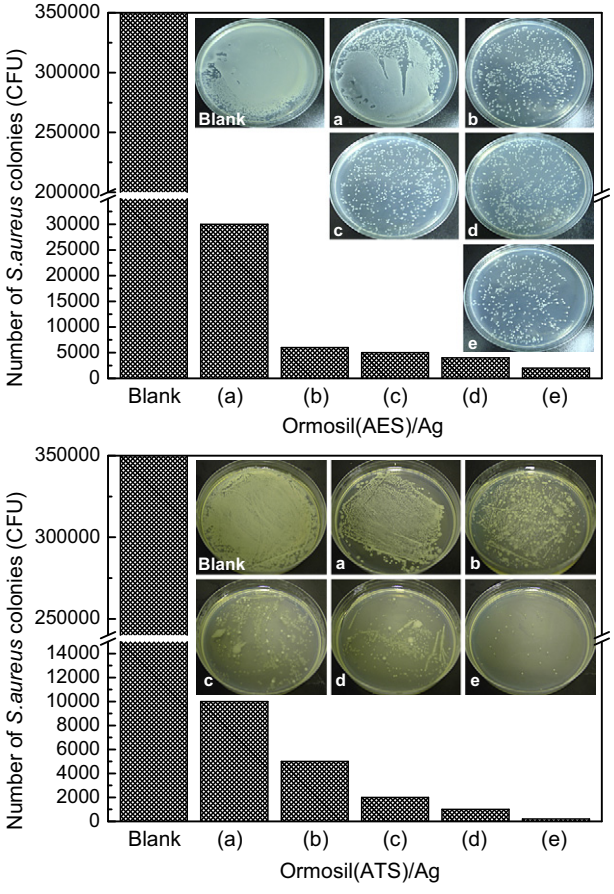


**Fig. 8.** Number of *S. aureus* colonies as a function of the weight of Ormosil(AES)/Ag (above) and Ormosil(ATS)/Ag (below) composites put into $10^7$ CFU of bacterial colonies. The inserted photograph of MH plates incubated under the condition in Fig. 8: (a) 10, (b) 20, (c) 30, (d) 40 and (e) 50 mg.

exhibited significant efficacy against bacteria of Gram class, especially against *B. subtilis*. After 24 h of incubation, the zones of inhibition of the Ormosil(ATS)/Ag composite against bacteria were significantly greater (17.93–30.09 mm) than those observed for the Ormosil(ATS) (16.27–26.39 mm), and were larger than that of the Ormosil(AES)/Ag composite (9.32–15.03 mm). From the above results, it could be concluded that the extent of coordination of $Ag^+$ ions by ATS was larger than that of the AES.

Fig. 8 shows the number of bacterial colonies grown on MH plates as a function of the amount of Ormosil/Ag composites when approximately $10^7$ CFU/mL of *S. aureus* were applied to the plates. Bacterial colonies grown on plates with more than 30 mg of Ormosil (ATS)/Ag particles were significantly smaller, and the antibacterial performance was greatly improved by increasing the amount of Ormosil(ATS)/Ag. Moreover, the antibacterial performance of the Ormosil(ATS)/Ag composite was larger than that of the Ormosil(AES)/Ag composite. As the high CFU levels applied in this study are rarely found in real-life systems, it appears that these Ormosil/Ag particles could possess an excellent biocidal effect and exhibit effectiveness in reducing bacterial growth. This result may be due to the uniform and fine distribution of silver particles on the surface of the Ormosil. The mechanism of the inhibitory action of silver ions on microorganisms is partially understood. It is believed that DNA loses its replication ability and cellular proteins become inactivated upon $Ag^+$ treatment [32]. In addition, it has also been shown that, following catalytic oxidation of silver ions with nascent oxygen, reaction takes place with bacterial cell membranes, leading to cell death [33].

## 4. Conclusions

The aminosilanes-modified silicate (Ormosil) was successfully used as a novel support for the immobilization of silver nanoparticles, and the effects of amine groups on the synthesis and antibacterial performance were also investigated. NMR, ESR, SEM, and TEM studies showed that the Ag particles were distributed uniformly on the Ormosil matrix. The aminosilanes-modified silicate acted as a superficial modifier and stabilizer of Ag nanoparticles, inhibiting their growth and preventing aggregation. These Ormosil/Ag composites possess excellent antibacterial abilities: its antibacterial performance against Gram-negative *E. coli* and *P. aeruginosa*, and Gram-positive *S. aureus* and *B. subtilis*, was investigated by zone of inhibition testing and the plate-counting method, and the results showed that the Ormosil/Ag composites exhibited strong antibacterial activity against these bacteria.

## Acknowledgements

The authors thank the Chung Shan Institute of Science and Technology for supporting this work. The authors express their gratitude to S.Y. Fang of the NSC Instrument Center for the NMR analysis.

## References

[1] Sanchez C, Julián B, Belleville PH, Popall M. Applications of hybrid organic–inorganic nanocomposites. J Mater Chem 2005;15:3559–92.
[2] Chou TP, Chandrasekaran C, Cao GZ. Sol–gel-derived hybrid coatings for corrosion protection. J Sol–Gel Sci Technol 2003;26(7):321–7.
[3] Metroke TL, Gandhi JS, Apblett A. Corrosion resistance properties of Ormosil coatings on 2024-T3 aluminum alloy. Prog Org Coat 2004;50(4):231–46.
[4] Maver K, Lavrenčič Štangar U, Judeinstein P, Zanotti JM. Dynamic studies of Ormosil membranes. J Non-Cryst Solids 2008;354(2):680–7.
[5] Lavrenčič Štangar U, Orel B, Vince J, Jovanovski V, Spreizer H, Šurca Vuk A, et al. Silicotungstic acid/organically modified silane proton-conducting membranes. J Solid State Electrochem 2005;9(2):106–13.
[6] Chakrabarti K, Whang CM. Silver doped ORMOSIL – an investigation on structural and physical properties. Mater Sci Eng B 2002;88(1):26–34.
[7] Sharma RK, Das S, Maitra A. Surface modified ormosil nanoparticles. J Colloid Interface Sci 2004;277(2):342–6.
[8] Laranjo MT, Stefani V, Benvenutti EV, Costa TMH, Ramminger GO, Gallas MR. Synthesis of ORMOSIL silica/rhodamine 6G: powders and compacts. J Non-Cryst Solids 2007;353(1):24–30.
[9] Frattini A, Pellegri N, Nicastro D, de Sanctis O. Effect of amine groups in the synthesis of Ag nanoparticles using aminosilanes. Mater Chem Phys 2005;94(1):148–52.
[10] Williams RL, Doherty PJ, Vince DG, Grashoff GJ, Williams DF. The biocompatibility of silver. Crit Rev Biocompat 1989;5(3):221–43.
[11] Slawson RM, Vandyke MI, Lee H, Trevors JT. Germanium and silver resistance, accumulation, and toxicity in microorganisms. Plasmid 1992;27(1):72–9.
[12] Spardaro JA, Chase SE, Webster DA. Bacterial inhibition by electrical activation of percutaneous silver implants. J Biomed Mater Res 1986;20:565–77.
[13] Russel AD, Hugo WB. Antimicrobial activity and action of silver. Proc Med Chem 1994;31:351–70.
[14] Gilchrist T, Healy DM, Drake C. Controlled silver-releasing polymers and their potential for urinary tract infection control. Biomaterials 1991;12(1):76–8.
[15] Joyce-Wöhrmann RM, Hentschel T, Münstedt H. Thermoplastic silver-filled poly-urethanes for antimicrobial catheters. Adv Eng Mater 2000;2(6):380–6.
[16] Shi Z, Neoh KG, Kang ET. Surface-grafted viologen for precipitation of silver nanoparticles and their combined bactericidal activities. Langmuir 2004;20:6847–52.
[17] Choi HJ, Han SW, Lee SJ, Kim K. Structure and thermal behavior of a layered silver hydroxyalkanecarboxylate. J Colloid Interface Sci 2003;264(2):458–66.
[18] Krklješ AN, Marinović-Cincović MT, Kacarevic-Popovic ZM, Nedeljković JM. Radiolytic synthesis and characterization of Ag–PVA nanocomposites. Eur Polym J 2007;43(6):2171–6.
[19] Wang H, Qiao X, Chen J, Ding S. Preparation of silver nanoparticles by chemical reduction method. Colloids Surf A 2005;256:111–5.
[20] Tian CG, Wang E, Kang ZH, Mao BD, Zhang C, Lan Y, et al. Synthesis of Ag-coated polystyrene colloids by an improved surface seeding and shell growth technique. J Solid State Chem 2006;179:3270–6.
[21] Luo CG, Zhang YH, Zeng XW, Zeng YW, Wang YG. The role of poly(ethylene glycol) in the formation of silver nanoparticles. J Colloid Interface Sci 2005;288:444–8.
[22] Chou CW, Hsu SH, Chang H, Tseng SM, Lin HR. Enhanced thermal and mechanical properties and biostability of polyurethane containing silver nanoparticles. Polym Degrad Stab 2006;91:1017–24.
[23] Li WG, Jia QX, Wang HL. Facile synthesis of metal nanoparticles using conducting polymer colloids. Polymer 2006;47:23–6.
[24] Wu KH, Yu PY, Hsieh YJ, Yang CC, Wang GP. Preparation and characterization of silver-modified poly(vinyl alcohol)/polyethyleneimine hybrids as a chemical and biological protective material. Polym Degrad Stab 2009;94:2170–7.
[25] Pandey PC, Upadhyay S, Tiwari I, Tripathi VS. An ormosil-based peroxide biosensor—a comparative study on direct electron transport from horseradish peroxidase. Sens Actuators B 2001;72:224–32.
[26] Pandey PC, Mishra AP. Novel potentiometric sensing of creatinine. Sens Actuators B 2004;99:230–5.
[27] Glaser RH, Wilkes GL, Bronnimann CE. Solid-state $^{29}Si$ NMR of TEOS-based multifunctional sol–gel materials. J Non-Cryst Solids 1989;113(1):73–87.
[28] Ivan S, Branka SS. Silver nanoparticles as antimicrobial agent: a case study on *E. coli* as a model for Gram-negative bacteria. J Colloid Interface Sci 2004;275:177–82.
[29] Khanna PK, Singh N, Charan S, Viswanath AK. Synthesis of Ag/polyaniline nanocomposite via an in situ photo-redox mechanism. Mater Chem Phys 2005;92:214–9.
[30] Yue ZX, Li LT, Zhou J, Zhang HG, Gui ZL. Preparation and characterization of NiCuZn ferrite nanocrystalline powders by auto-combustion of nitrate–citrate gels. Mater Sci Eng B 1999;64:68–72.
[31] Yang FC, Wu KH, Liu MJ, Lin WP, Hu MK. Evaluation of the antibacterial efficacy of bamboo charcoal/silver biological protective material. Mater Chem Phys 2009;113:474–9.
[32] Feng QL, Wu J, Chen GQ, Cui FZ, Kim TN, Kim JQ. A mechanistic study of the antibacterial effect of silver ions on *Escherichia coli* and *Staphylococcus aureus*. J Biomed Mater Res 2000;52(4):662–8.
[33] Li P, Li J, Wu CZ, Wu QS, Li J. Synergistic antibacterial effects of β-lactam antibiotic combined with silver nanoparticles. Nanotechnology 2005;16:1912–7.